Journal of Sound and Vibration 595 (2025) 118744

Contents lists available at ScienceDirect

Journal of Sound and Vibration

journal homepage: www.elsevier.com/locate/jsvi

Atypical second harmonic A0 mode Lamb waves in non-uniform plates for local incipient damage monitoring

Shengbo Shan [a,b,*], Gujun Wu [a], Ze Liu [c], Yuanman Zhang [c], Li Cheng [c,d,*]

[a] School of Aerospace Engineering and Applied Mechanics, Tongji University, Shanghai, 200092, PR China
[b] Shanghai Institute of Aircraft Mechanics and Control, Shanghai, 200092, PR China
[c] Department of Mechanical Engineering, The Hong Kong Polytechnic University, Kowloon, Hong Kong
[d] Hong Kong Branch of National Rail Transit Electrification and Automation Engineering Technology Research Center, The Hong Kong Polytechnic University, Kowloon, Hong Kong

ARTICLE INFO

Keywords:
Lamb waves
Second harmonic
A0 mode waves
Non-uniform plate
Incipient damage

ABSTRACT

Plates with non-uniform thickness, such as stiffened and notched plates, are commonly seen in engineering applications. Monitoring incipient damage in these structures is crucial to ensure their safety during service. Second harmonic Lamb waves hold great promise for structural health monitoring applications. However, the mechanisms underpinning the generation of the second harmonic Lamb waves in non-uniform plates are still not well understood due to the complex wave field. To tackle this issue, a theoretical analysis is first conducted to highlight the so-called atypical second harmonic A0 mode waves (2nd A0 waves) generated at the structural non-uniform section. Their existence, as well as their potential for local incipient damage monitoring applications, is then confirmed by finite element simulations. Experiments are carried out on a notched aluminum plate to monitor the incipient plastic damage induced by bending. Three mechanisms contributing to the generation of the atypical 2nd A0 waves in the non-uniform plate are identified: mode conversion from the second harmonic S0 mode waves, asymmetric nonlinear driving forces at the non-uniform section, and the mutual interaction between the mode-converted fundamental A0 and S0 waves. This study shows that the reported atypical 2nd A0 waves provide an effective means for monitoring local incipient damage in non-uniform structures.

1. Introduction

Recent advances in structural health monitoring (SHM) have made it possible to detect incipient damage in structures, which greatly facilitate maintenance decision making. Incipient damage typically manifests in structures as material nonlinearity that degrades before the onset of macro defects [1-3]. When interacting with material nonlinearity, guided waves generate nonlinear components such as higher harmonics, mixed-frequency components, nonlinear static components, *etc.* [4-10]. Given their appealing features and high sensitivity to incipient damage, nonlinear guided waves in thin-walled structures have gained increasing interest in recent years [11,12].

Among various types of nonlinear guided waves, the second harmonic Lamb waves have been extensively studied and utilized for

* Corresponding authors.
E-mail addresses: shanshengbo@tongji.edu.cn (S. Shan), li.cheng@polyu.edu.hk (L. Cheng).

https://doi.org/10.1016/j.jsv.2024.118744
Received 3 April 2024; Received in revised form 12 September 2024; Accepted 16 September 2024
Available online 18 September 2024

SHM applications [13-17]. As a prerequisite, it is essential to comprehend their generation and propagation characteristics. Previous studies have demonstrated that the second harmonic Lamb waves can only be generated when there is a non-zero power flux from the fundamental waves to the second harmonic waves [18,19]. This means that only symmetric second harmonic Lamb waves can be generated in a symmetric plate with a neutral plane, regardless of whether the fundamental waves are symmetric or antisymmetric. Additionally, if the phase velocities between the fundamental and second harmonic waves match, the resultant second harmonic Lamb waves can accumulate over the traveling distance [20,21]. Recently, second harmonic A0 mode waves (2nd A0 waves) were found in a PZT-activated system due to the mixing of the primary S0 and A0 waves, which provides an appealing alternative for SHM in terms of both detection and localization [22,23].

Based on the acquired understanding, many SHM applications have been materialized [3,24,25]. For example, Li et al. applied a reconstruction algorithm for the probability inspection using the second harmonic S0 mode Lamb waves to locate micro-defects in a 1060 aluminum plate [26]. The S2-S4 mode pair was utilized to evaluate tensile damage and microstructural evolution of AISI 316 L steel [27]. The work demonstrated a correlation between the second harmonic waves and the material microstructural changes during plastic deformation. Based on the generation mechanisms of the 2nd A0 wave, our previous work proposed a detection and localization strategy for incipient damage using an example of thermal damage in aluminum 2024-T3 plates [23].

Previous efforts mostly focused on uniform plates. Engineering structures, however, often contain non-uniform sections, such as stiffeners or notches, which are often more susceptible to damage. To develop relevant SHM techniques, it is essential to understand the generation and propagation characteristics of second harmonic Lamb waves in these types of structures. Some existing studies investigated the reflections and transmissions of linear guided waves at non-uniform sections [28-30]. In particular, Pagneux proposed an analytical framework to calculate the scattering features of Lamb waves in plates with continuously varying thickness [31]. Feng and Schaal further studied the scattering of Lamb waves at the structural discontinuity using the mode decomposition method [32,33]. Zima and Moll conducted numerical and experimental investigations on guided wave propagation in aluminum plates with specially designed thicknesses [34]. By contrast, research on nonlinear guided waves in non-uniform plates is relatively scarce due to the complex wave phenomena caused by wave reflections and transmissions at the non-uniform section. In this regard, Skidar et al. proposed a deep learning-based method for assessing breathing disbonds in stiffened composite panels using nonlinear guided waves [35]. Similarly, Mandal and Banerjee designed an active sensing technique to identify breathing disbonds in stiffened metallic plates with nonlinear Lamb waves [36]. Both methods, however, put strong emphasis on signal processing with little attention paid to exploring the underlying mechanisms of nonlinear guided waves in such structures. Recently, Zuo et al. proposed a theoretical framework for analyzing the propagation and scattering characteristics of the second harmonic Lamb waves in a discontinuous plate subjected to primary S0 mode Lamb wave incidence [37]. While the generation of 2nd A0 waves was numerically observed in that study, the underlying mechanisms remain unclear. Therefore, there is still a general lack of thorough understanding of nonlinear guided wave generation mechanisms in non-uniform plates. This hampers SHM applications in terms of selecting the appropriate Lamb wave mode and frequency, as well as interpreting the response signals.

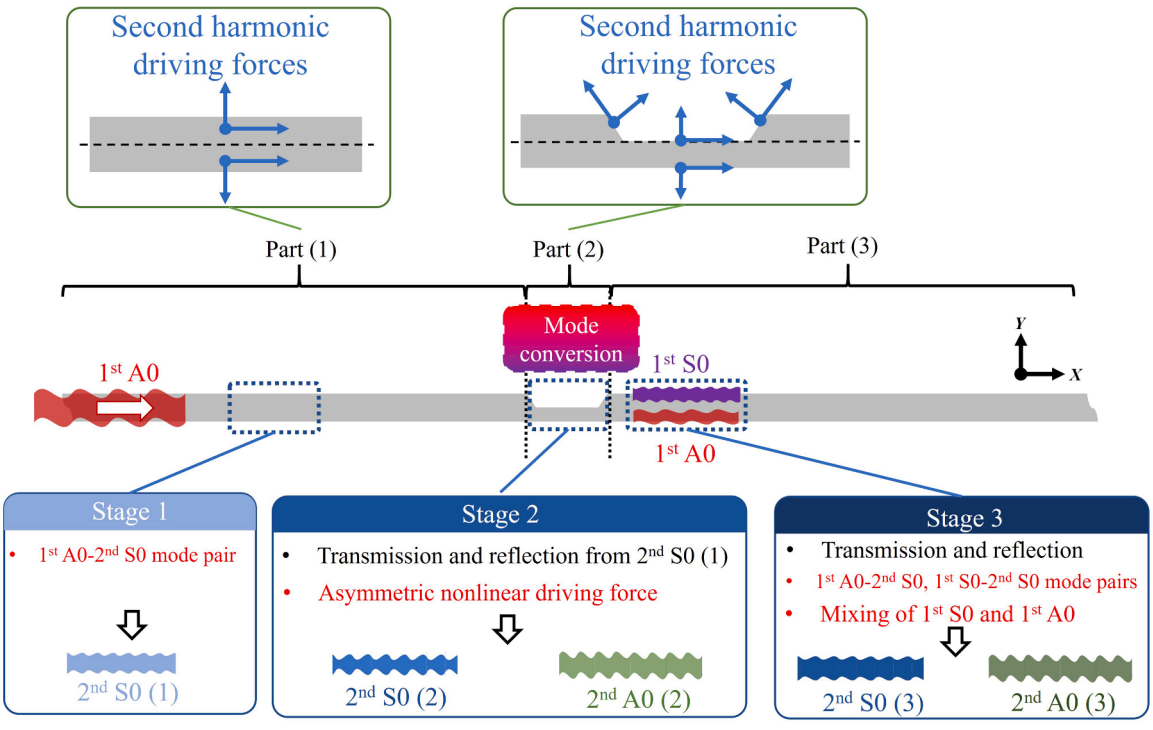

Fig. 1. Concept of the second harmonic A0 wave generation.

Motivated by the above issues, this work investigates the generation mechanism of the second harmonic Lamb waves in non-uniform plates, specifically highlighting the so-called atypical 2nd A0 waves generated at the structural non-uniform section. Theoretical analyses are conducted to ascertain the generation mechanisms of the 2nd A0 waves, which are then confirmed by finite element simulations and experiments. The potential of the observed atypical 2nd A0 waves for local incipient damage monitoring applications is finally assessed from the SHM perspective.

2. Mechanism of the second harmonic A0 wave generation in a non-uniform plate

Consider an incident A0 mode Lamb wave propagating in a non-uniform aluminum plate, exemplified by a notched plate as shown in Fig. 1. When the incident wave encounters the notch, mode conversion takes place, thus generating the S0 and A0 mode Lamb waves at the fundamental frequency (referred to as 1st A0 and S0 waves, respectively). This section explains how fundamental waves interact and generate nonlinear waves in a plate with weak material nonlinearity. It briefly recaps the basic theory of nonlinear Lamb wave generation in a uniform plate, followed by subsequent analyses of the second harmonic nonlinear wave generation in a non-uniform plate.

2.1. Nonlinear Lamb wave generation in a uniform plate

The Landau-Lifshitz model is used to characterize the weak material nonlinearity of the plate, by taking into account the quadratic nonlinearity as [38]

$$\mathbf{T} = \lambda tr[\mathbf{E}]\mathbf{I} + 2\mu\mathbf{E} + \overline{A}\mathbf{E}^2 + \overline{\mathrm{B}}tr\left[\mathbf{E}^2\right]\mathbf{I} + 2\overline{\mathrm{B}}tr[\mathbf{E}]\mathbf{E} + \overline{C}(tr[\mathbf{E}])^2, \tag{1}$$

where λ and μ are Lamé constants and $\overline{A}$, $\overline{\mathrm{B}}$, $\overline{C}$ are the Landau third-order elastic constants. The second rank identity tensor is represented by **I**. The operation $tr[]$ is the trace. The second Piola-Kirchhoff stress and Lagrangian stain tensors are denoted by **T** and **E**, respectively. Specifically, the Lagrangian stain tensor is related to the displacement gradient, $\mathbf{H} = \nabla\mathbf{u}$, as

$$\mathbf{E} = \frac{1}{2}\left(\mathbf{H} + \mathbf{H}^{\mathrm{T}} + \mathbf{H}^{\mathrm{T}}\mathbf{H}\right). \tag{2}$$

The first Piola-Kirchhoff stress **P** is then introduced which is further decomposed to the linear and nonlinear parts as

$$\mathbf{P}(\mathbf{H}) = (\mathbf{I} + \mathbf{H})\mathbf{T}(\mathbf{H}) = \mathbf{P}^{\mathbf{L}}(\mathbf{H}) + \mathbf{P}^{\mathbf{NL}}(\mathbf{H}). \tag{3}$$

The superscripts "**L**" and "**NL**" denote the linear and nonlinear parts, respectively.

Without loss of generality, assume two Lamb waves *a* and *b* propagating in a uniform plate with a thickness of 2 h in the *X* direction. Their wavefields in terms of the displacement **u** write

$$\mathbf{u}_a(X, Y, t) = \frac{1}{2}A_a\mathbf{U}_a(Y)\mathrm{e}^{i(k_aX - \omega_a t)} + c.c., \tag{4a}$$

$$\mathbf{u}_b(X, Y, t) = \frac{1}{2}A_b\mathbf{U}_b(Y)\mathrm{e}^{i(k_bX - \omega_b t)} + c.c., \tag{4b}$$

where $\mathbf{U}(Y)$ denotes the wave structure (mode shape) in terms of the displacement across the plate thickness in the *Y* direction. The wavenumber and angular frequency are denoted by k and ω, respectively. A is the modal amplitude and *c.c.* represents the complex conjugate.

The interaction between the fundamental waves and the quadratic material nonlinearity generates the nonlinear Lamb waves. According to the normal mode expansion technique [18,19], the nonlinear Lamb waves in terms of the displacement $\mathbf{u}^{(2)}$ can be expressed as a summation of all Lamb wave modes m as

$$\mathbf{u}^{(2)}(X, Y, t) = \frac{1}{2}\sum_{m=1}^{\infty} A_m(X)\mathbf{U}_m(Y)\mathrm{e}^{-i(\omega_a \pm \omega_b)t} + c.c.. \tag{5}$$

The superscript "$^{(2)}$" indicates the nonlinear waves relating to quadratic nonlinearity. By applying the perturbation theory and normal model expansion technique, the amplitude of the m^{th} mode nonlinear Lamb wave (A_m) is governed by

$$4P_{mm}\left(\frac{\mathrm{d}}{\mathrm{d}X} - ik_m{}^*\right)A_m(X) = \left(f_m^{\mathrm{surf}} + f_m^{\mathrm{vol}}\right)e^{i(k_a \pm k_b)X}, \tag{6}$$

where

$$P_{mm} = -\frac{1}{4}\int_{-h}^{h}\left(\frac{\mathbf{P}_m\mathbf{v}_m^* + \mathbf{P}_m^*\mathbf{v}_m}{4}\right)\cdot\mathbf{n}_X\,\mathrm{d}Y, \tag{7}$$

$$f_m^{\text{surf}} = -\frac{1}{2}\mathbf{v}_m^* \mathbf{P}^{\mathbf{NL}} \cdot \mathbf{n}_Y \Big|_{-h}^{h}, \tag{8}$$

$$f_m^{\text{vol}} = \frac{1}{2}\int_{-h}^{h} \nabla \mathbf{P}^{\mathbf{NL}} \cdot \mathbf{v}_m^* \mathrm{d}Y. \tag{9}$$

In the above equations, $\mathbf{n_X}$ and $\mathbf{n_Y}$ are the unit vectors along the X and Y directions, respectively. The superscript * denotes the complex conjugate. Specifically, $\mathbf{P}^{\mathbf{NL}}$ is obtained by substituting the linear wave field quantities into Eq. (3) according to the perturbation theory. f_n^{surf} and f_n^{vol} are the surface and volume nonlinear driving terms that add up to the power flux from the primary waves to the nonlinear wave. The solution to Eq. (6) writes

$$A_m(X) = \frac{f_n^{\text{surf}} + f_n^{\text{vol}}}{4P_{mn}} \begin{cases} \dfrac{i}{k_n^* - 2k}\left(e^{i(k_a \pm k_b)X} - e^{ik_m^* X}\right), & k_m^* \neq k_a \pm k_b \\ Xe^{i(k_a \pm k_b)X}, & k_m^* = k_a \pm k_b \end{cases} \tag{10}$$

Eq. (10) shows that the generation of the nonlinear waves necessitates the non-zero power flux from the fundamental waves to the nonlinear wave. Additionally, if the phase velocity of the primary waves and that of the nonlinear Lamb wave match, the resultant nonlinear Lamb wave accumulates over the propagation distance.

As a special case, when considering only the self-interaction of a specific wave or the mutual interaction of two modes of waves at the same fundamental frequencies ($\omega_a = \omega_b$), the second harmonic waves are generated. This provides the foundation for subsequent analyses.

2.2. Second harmonic Lamb wave generation in a non-uniform plate

As shown in Fig. 1, the notched plate is divided into three parts, and the process of nonlinear guided wave generation can also be divided into the following three stages accordingly.

Stage 1: When the 1st A0 mode Lamb wave propagates in Part 1, it generates a second harmonic Lamb wave. However, based on the power flux requirement from Eqs. (8) and (9), only the 2nd S0 wave is generated due to the symmetric nonlinear driving forces. As the velocities of A0 and S0 mode Lamb waves significantly differ in the low-frequency range (exemplified in Fig. 2), the generated 2nd S0 wave is not cumulative.
Stage 2: The generated 2nd S0 wave in Stage 1 propagates and encounters the notch in Part 2, thus causing mode conversion and generation of the 2nd A0 wave. In addition, the 1st A0 wave causes asymmetric nonlinear diving forces due to the material nonlinearity when it reaches the notch. These forces further excite the 2nd S0 and 2nd A0 waves in the plate.
Stage 3: The second harmonic components generated in Part 1 and Part 2 are further transmitted and reflected at the left edge of Part 3, resulting in the generation of the 2nd A0 waves. Additionally, when the primary waves reach Part 3, both the 1st S0 and 1st A0 waves are present. Power flux analyses stipulate that the self-interaction of the 1st S0 and 1st A0 waves generates the 2nd S0 waves. Meanwhile, the mutual interaction between the 1st S0 and 1st A0 waves also exists, leading to the generation of the 2nd A0 waves [22].

Therefore, the 1st A0 waves in a uniform plate only generate the 2nd S0 waves, but also the 2nd A0 waves in a non-uniform plate, which is therefore called atypical 2nd A0 waves. Furthermore, the non-uniform section generates the 2nd A0 waves through three different mechanisms: 1) the mode conversion from the 2nd S0 waves; 2) the resultant asymmetric nonlinear driving forces at the non-uniform section; and 3) the mutual interaction between the mode-converted fundamental A0 and S0 waves. Despite the complexity of these mechanisms, the 2nd A0 waves are directly related to the non-uniform section. This might be capitalized for monitoring local incipient damage in non-uniform structures as to be demonstrated in later sections.

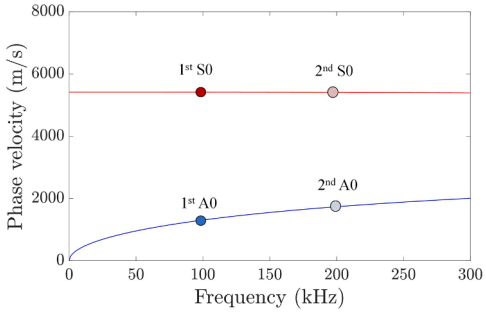

Fig. 2. Dispersion curves of Lamb waves in a 2-mm thick aluminum plate.

3. Numerical validations and explorations

Finite element investigations are carried out to confirm the theoretically predicted 2nd A0 waves in a non-uniform plate and to explore their potential for incipient damage monitoring applications. In principle, when the 1st A0 waves interact with the non-uniform section of a structure, asymmetric nonlinear driving forces are elicited, leading to the generation of atypical 2nd A0 waves. In light of this phenomenon, we believe that the proposed methodology can be adapted for the monitoring of plates with either notches or stiffeners. In this work, a representative notched plate is studied and modeled using Abaqus, as shown in Fig. 3. The plate has a uniform thickness of 2 mm, except for the notched part, where the thickness is reduced to 1 mm. The total length of the plate is 600 mm, and the length of the notch is 20 mm. A prescribed displacement with an amplitude of 100 nm is applied to the left edge for the A0 wave excitation. The excitation signal is a 5-cycle tone burst signal windowed by a Hann function at a central frequency of 100 kHz. The model employs plane strain elements (CPE4) that are 0.5 mm $\times$ 0.5 mm in size, ensuring >20 elements per smallest wavelength under consideration. Material nonlinearity is introduced to the model via a user-material subroutine (UMAT).

Aluminum is used with a mass density of 2700 kg/m^3. To ascertain the mechanisms of 2nd A0 wave generation, three different sets of elastic constants are considered, as shown in Table 1 [23]. The plate is also divided into three parts, having different material properties as detailed in the subsequent analyses.

3.1. Observation of the second harmonic A0 waves

The generation of the atypical 2nd A0 waves in the non-uniform plate (NP) is first verified. A benchmark is used with a uniform plate (UP) that has the same dimensions as the non-uniform plate but without the notch. Both plates are made of nonlinear aluminum (NAL). The out-of-plane displacements (U_Y) at position P2 (50 mm away from the right end of the notch as marked in Fig. 3) are used as the system output. Fig. 4(a) illustrates the linear responses at the top surface of the plate, which show similar amplitudes of the 1st A0 waves. To extract the nonlinear responses, the phase-inverse method is applied by superimposing the responses to a pair of excitation signals with inversed phases [13,39]. The extracted nonlinear responses for the uniform and non-uniform plates are plotted in Fig. 4 (b). In addition to the second harmonic responses, strong nonlinear static components are also observed. To isolate the second harmonic responses and mitigate the influence of the static components on the analyses, a Butterworth filter with a passband from 150 kHz to 250 kHz is deployed. The processed results are presented in Fig. 4(c), showing that the second harmonic response from the non-uniform plate is much stronger than that from the uniform plate. It is worth noting the response from the uniform plate is attributed to the 2nd S0 waves. To verify this, the responses at the top and bottom surfaces at P2 are superimposed to eliminate the S0 mode components. As a result, the extracted 2nd A0 waves are obtained in Fig. 4(d). It shows no 2nd A0 waves in the uniform plate, while the atypical 2nd A0 waves are generated in the non-uniform plate, consistent with the theoretical prediction. According to the literature [26], non-classical acoustic contact nonlinearity (CAN) responsible for second harmonic generation is not applicable when the defect size significantly exceeds the wave amplitude. In this case, the notch width of 20 mm is substantially greater than the wave amplitude of approximately 100 nm. Consequently, no CAN will transpire for the production of the second harmonic waves in the present cases.

3.2. Mechanisms of second harmonic A0 wave generation

The mechanisms of the 2nd A0 wave generation are studied by attributing the NAL to the three parts separately while assigning the other parts with LAL (see the caption of Table I for the definition of NAL, LAL, and DAL). The contribution of the three parts to the generated 2nd A0 waves is assessed. Fig. 5(a) shows the 2nd A0 waves at P2 resulting from the three different parts. A window is selected in accordance with 1st A0 waves, and the amplitudes of the wave packets in the selected window are further extracted in Fig. 5 (b). It is evident that the nonlinearity at the notch overwhelms the resultant 2nd A0 waves. This indicates that the 2nd A0 waves are highly effective in monitoring damage on the notch in the non-uniform plate.

3.3. Applications of the second harmonic A0 waves

In practical applications, it is necessary to effectively measure the 2nd A0 waves generated at the notch to monitor the incipient damage. To verify this, the responses are extracted before and after the notch at P1 and P2, as shown in Fig. 6. In the simulation, NAL is assigned to the entire plate. The amplitudes of the linear A0 waves change slightly after passing through the notch, as shown in Fig. 6 (a). In comparison, the amplitudes of the 2nd A0 waves increase sharply after passing through the notch in Fig. 6(b). Theoretical analyses suggest that when the 1st A0 waves encounter the non-uniform section of the plate, asymmetric nonlinear driving forces are

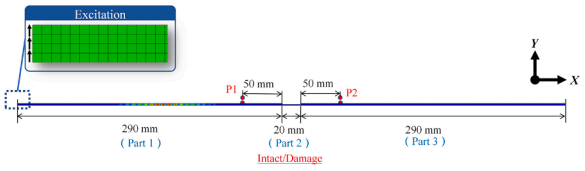

Fig. 3. Finite element model.

Table 1
Elastic constants of materials in the simulations (Units: GPa).

Materials*	λ	μ	$\overline{A}$	$\overline{B}$	$\overline{C}$
LAL	55.27	25.95	0	0	0
NAL	55.27	25.95	−351.2	−140.4	−102.8
DAL	55.27	25.95	−1053.6	−521.2	−308.4

* LAL: linear aluminum, NAL: nonlinear aluminum, DAL: damaged aluminum.

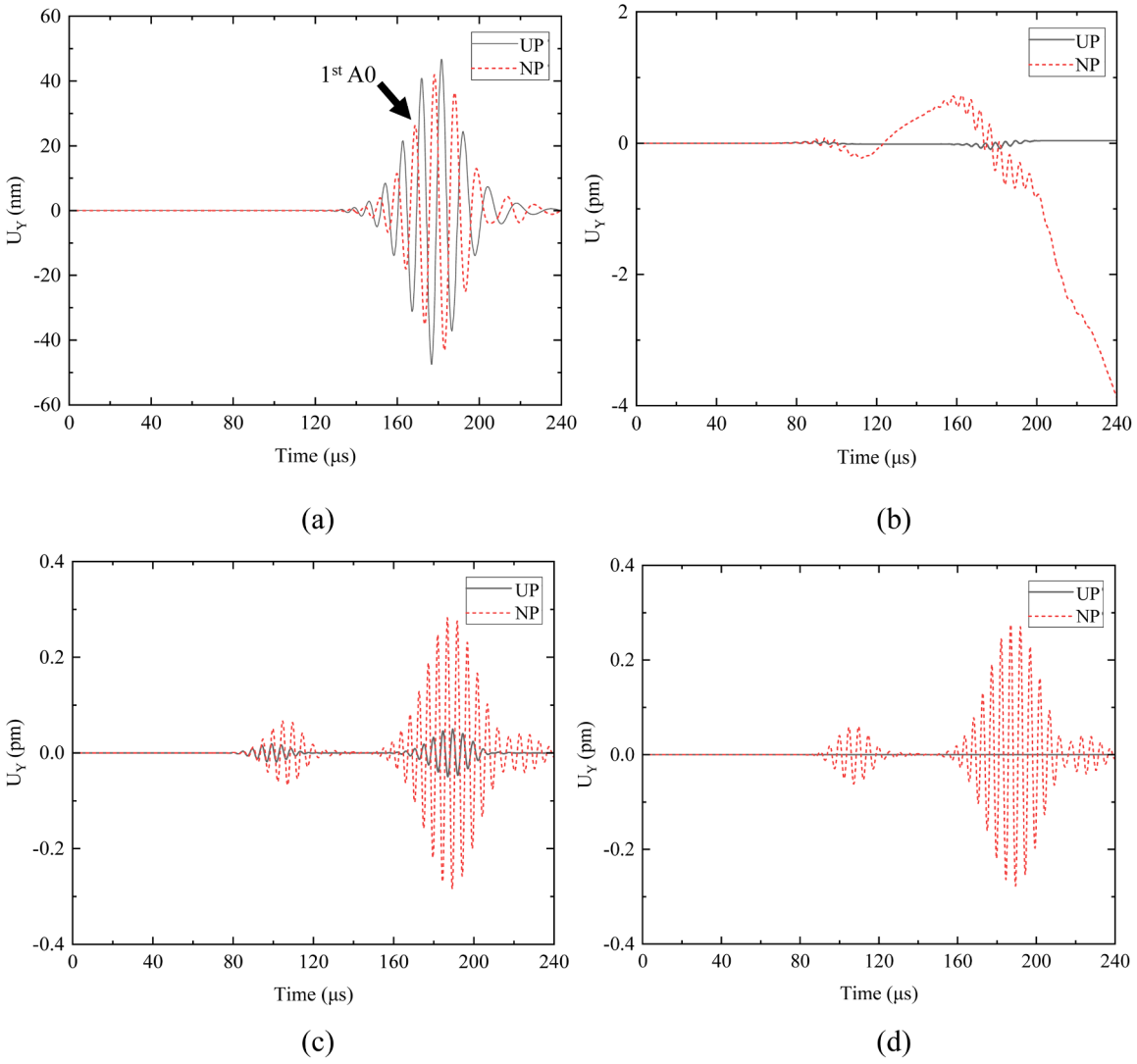

Fig. 4. Out-of-plane responses captured at P2 in the uniform plate (UP) and non-uniform plate (NP): (a) linear responses; (b) extracted nonlinear responses; (c) filtered second harmonic responses; (d) extracted second harmonic A0 responses.

elicited to generate the 2nd A0 waves propagating in both forward and backward directions. Consequently, the wave packets observed in the nonlinear responses at approximately 180 μs captured at both P1 and P2 are attributed to the 2nd A0 waves generated at the non-uniform section. More importantly, this confirms the dominance of the material nonlinearity at the notch in the captured 2nd A0 waves at P2.

Finally, the feasibility of using the 2nd A0 waves for incipient damage monitoring is demonstrated. The intact plate is assigned with NAL. For the damaged plate, the damaged aluminum (DAL) is assigned to Part 2 of the non-uniform plate with varying Landau constants while the remaining parts are still NAL. Fig. 7 shows the 1st and 2nd A0 waves captured at P2. The 1st A0 wave hardly changes by the incipient damage (Fig. 7(a)), while the 2nd A0 wave increases significantly (Fig. 7(b)). This confirms the efficacy of the 2nd A0 waves for local incipient damage monitoring in non-uniform plates. In addition, relatively weak wave packets appear at around

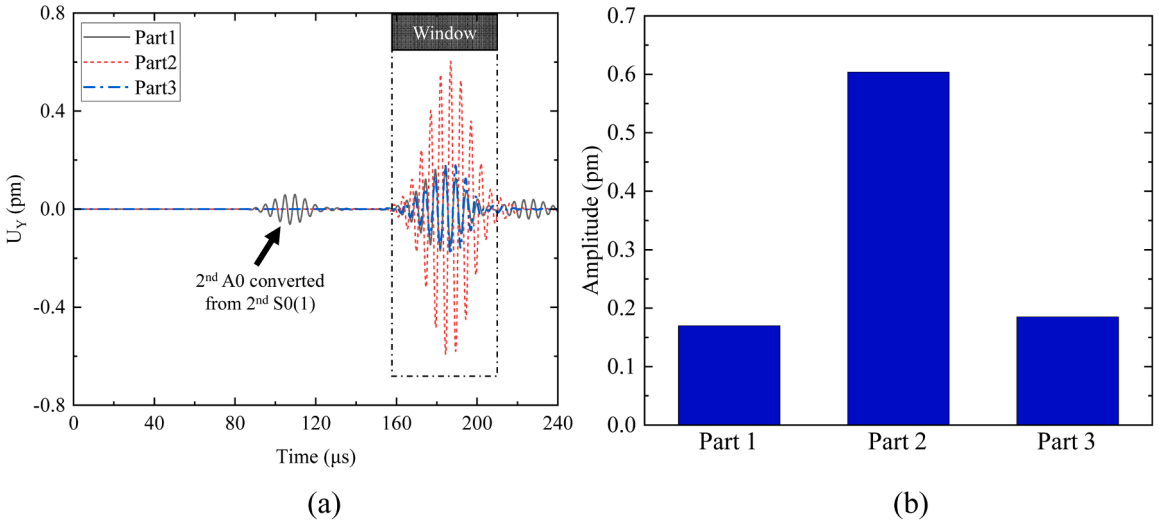

Fig. 5. (a) Second harmonic A0 mode responses captured at P2 in the non-uniform plate considering the material nonlinearity from three parts; (b) extracted amplitudes of waves in the window.

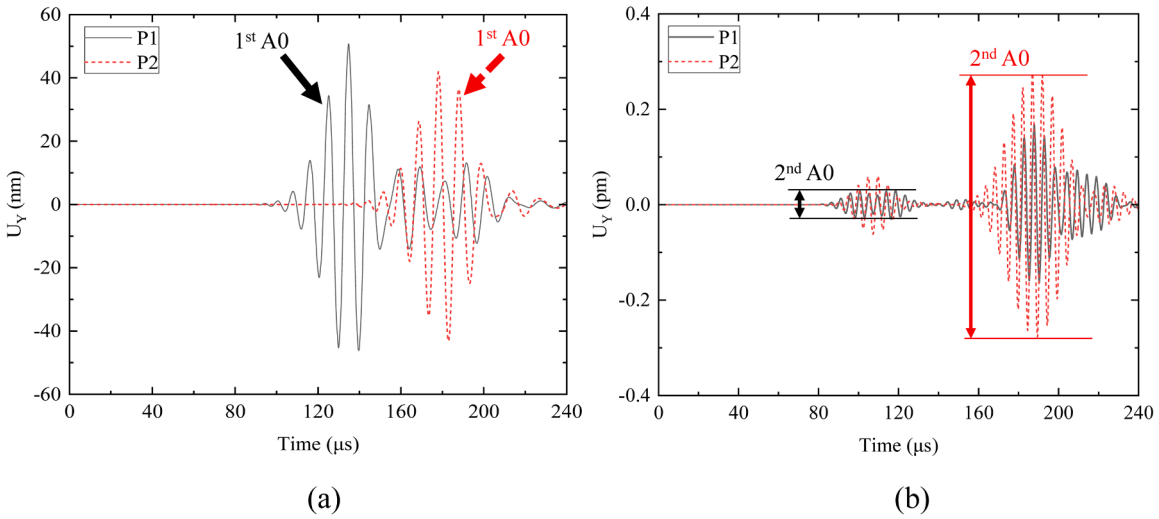

Fig. 6. The (a) linear and (b) second harmonic A0 mode responses captured at P1 and P2 in the non-uniform plate.

100μs for the nonlinear responses which are associated with the 2nd A0 wave converted from the 2nd S0(1) wave. Since mode conversion is primarily due to linear wave transmissions, the introduction of incipient damage via ToECs changes has minimal impact on the linear features of the guided waves. This further substantiates our theoretical analyses from a different perspective.

4. Experimental validations and applications

Experiments are conducted to validate the predicted 2nd A0 wave generation in non-uniform plates before applying to local incipient damage monitoring. To this end, two 2024-T3 aluminum plates measuring 600 mm × 200 mm × 2 mm are tested, as shown in Fig. 8(a). The non-uniform plate has a 20mm-wide and 1mm-deep notch. Two measurement points, P1 and P2, are selected at a distance of 50 mm from the edges of the notch, in accordance with the simulations. PZT actuators, 30 mm × 8 mm × 0.5 mm, are bonded on the plate, 200 mm away from the notch. The measurement system is illustrated in Fig. 8(b). A controller generates an excitation signal to the National Instruments (NI) PXIe-5423 signal generator. The excitation signal is a 5-cycle tone burst signal with a central frequency of 100 kHz. A T&C AG1020 power amplifier amplifies the output signal to 3 W, feeding the PZT actuator to generate Lamb waves in the plates. The Lamb waves are captured by an air-coupled sensor with a frequency of 200 kHz and liftoff of around 45 mm. The signals are then amplified by the PXPA6 preamplifier and recorded by the NI PXIe-5105 data acquisition module. During the test, the sensor remains fixed while the plate is moved to measure the responses at P1 and P2. In each test, 200 measurements are taken

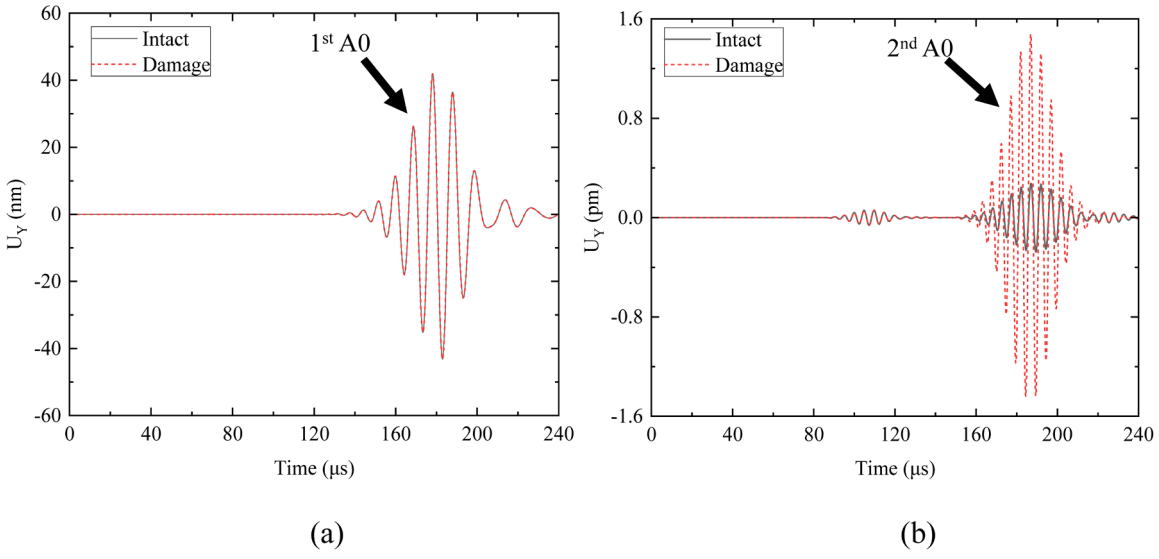

Fig. 7. The (a) linear and (b) second harmonic A0 mode responses captured at P2 in the non-uniform plate before and after damage is introduced to Part 2.

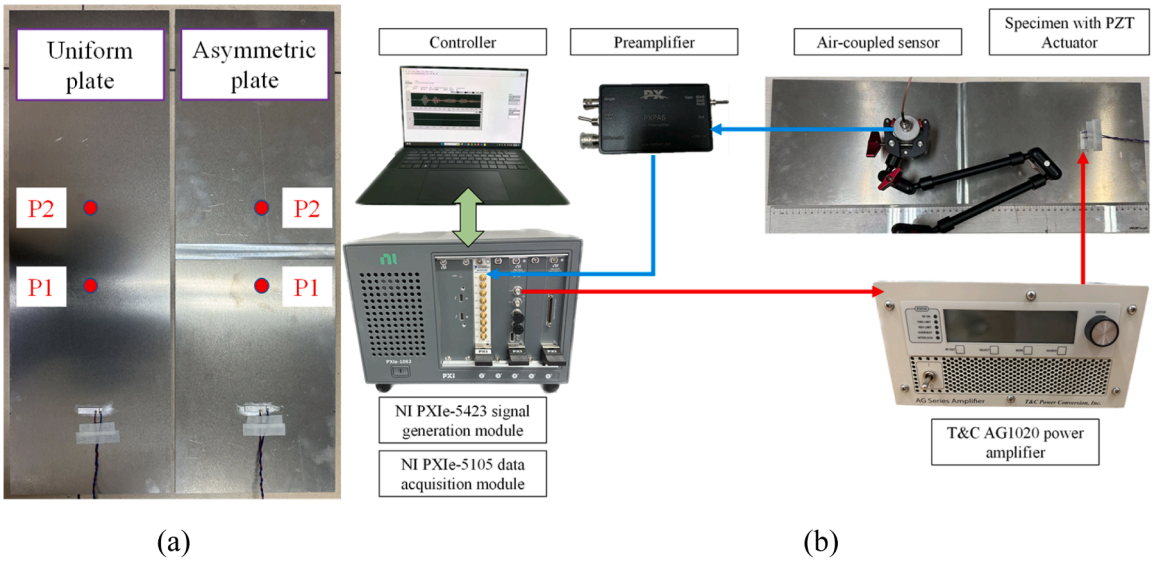

Fig. 8. (a) The specimens with actuators and (b) the experimental setup.

and the responses are averaged to reduce the noise effect and uncertainties.

4.1. Experimental validation

The 2nd A0 wave generation due to the notch is first validated through comparisons with benchmark uniform plate. The responses captured at P1 and P2 in the uniform plate are presented in Fig. 9. The linear A0 waves are highlighted in the windows in Fig. 9(a), showing a slight attenuation with respect to wave propagation distance. The second harmonic responses are then extracted using the phase-inverse method and filtered with the Butterworth filter, as shown in Fig. 9(b). Different from the simulations, the PZT actuator excites both the 1st S0 and A0 mode waves. Their mutual interaction leads to the generation of the 2nd A0 waves in the uniform plate [22]. According to the wave velocities, the wave packets associated with the 2nd A0 waves are highlighted. The attenuation pattern of the 2nd A0 waves with respect to the wave propagation distance is also exhibited.

By comparison, the linear and nonlinear responses in the non-uniform plate are plotted in Fig. 10. The 1st A0 mode waves exhibit a decaying tendency during propagation (Fig. 10(a)), while the 2nd A0 waves show a significant increase after passing through the notch

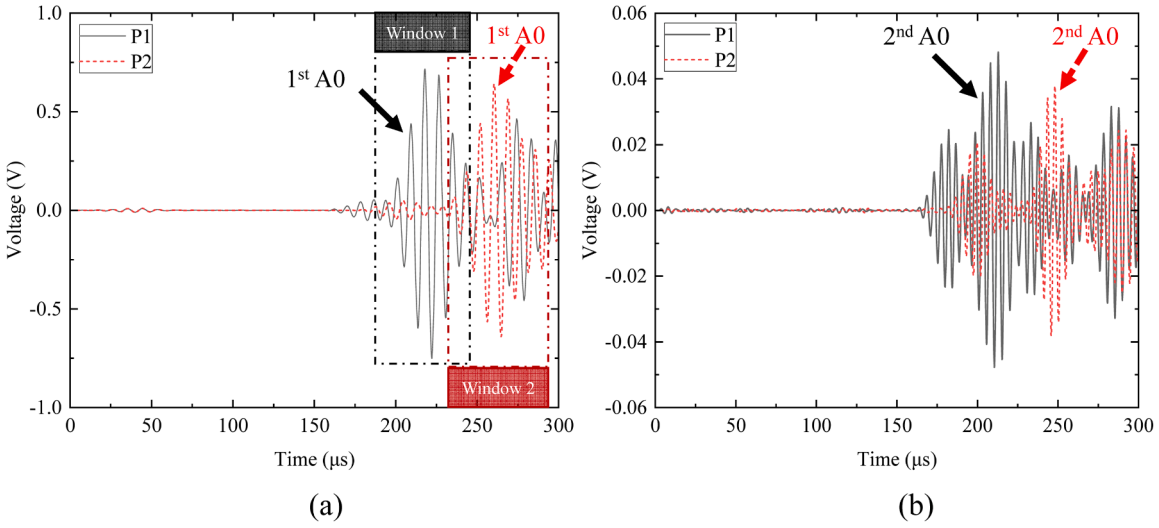

Fig. 9. The (a)linear and (b)second harmonic responses captured at P1 and P2 in the uniform plate.

(Fig. 10(b)).

Remarkably, S0 mode Lamb waves can also be generated by the PZT actuator, which adds complexity to both the wave field and the response signals. However, we employed an air-coupled sensor to capture the responses, which is a device for capturing the out-of-plane vibrations of the plate. The particular configuration allows for reducing the influence of the S0 mode waves on the results. The captured linear wave responses in Fig. 10(a) also show the dominance of the A0 mode Lamb waves. Furthermore, due to the significant differences in group velocities between the S0 and A0 mode Lamb waves at 200 kHz, the wave packets associated with the 2nd A0 waves are distinctly recognizable in the response signals. This distinction further helps in minimizing the impact of the S0 mode waves on the results.

A relative nonlinearity parameter (β') is then defined to quantify the nonlinearity level at different locations in the two plates as

$$\beta' = \frac{\sqrt{\int_{t_1}^{t_2} \left(S^{NL}(t)\right)^2 \mathrm{d}t}}{\int_{t_1}^{t_2} \left(S^{L}(t)\right)^2 \mathrm{d}t} \tag{11}$$

where S^{NL} and S^{L} are the linear and nonlinear response signals respectively. t_1 and t_2 represent the start and stop time of the selected window, respectively. The window length is equal to the duration of the excitation signals, with its center being chosen as the time with the highest amplitude of the wave packet. Measurements are repeated five times, and the error bars are calculated to ensure result consistency. The results are obtained in Fig. 11 by normalizing with respect to the β' measured at P1 in the uniform plate The experiments confirm a significant increase in β' after the waves pass the notch, indicating effective measurement of the 2nd A0 waves generated by the notch.

4.2. Application for local incipient damage monitoring

Monitoring of local incipient damage is attempted using the 2nd A0 waves. To generate local plasticity at the notch, the plate is bent first to 145° on one side and then to −145° on the other side, before resuming to its original flat state as shown in Fig. 12. This entire process is considered one bending cycle. During the experiments, five bending cycles are performed, and the 2nd A0 waves are measured to monitor the changes in the material nonlinearity at the notch. Specifically, ultrasonic tests are conducted four times after each bending operation. For each test, we reposition the plate and carry out the ultrasonic measurement to calculate the β' value. The standard deviation is subsequently utilized to quantify the error bar, providing a statistical measure of the variability in the data.

As an example, Fig. 13 presents the linear and nonlinear responses captured at P2 before and after the first bending cycle. The 1st A0 waves show marginal changes, while the 2nd A0 waves vary significantly. This confirms that the 2nd A0 waves indeed have a much higher sensitivity to local incipient damage than their linear counterparts. Fig. 14 shows the calculated β' corresponding to different bending cycles, normalized with respect to the intact case. The normalized β' generally exhibits an increasing and then decreasing trend, consistent with previous literature [40,41]. It is worth noting that the non-contact air-coupled sensor was utilized to capture the waves. Despite our effort in using markers to position the plate, slight variations in measurement positions among the four tests could occur. This may contribute to the relatively high variance in the error bars in Fig. 14. Nevertheless, we believe the observed evolution trend of β' throughout the bending process can still accurately reflect the material degradation, thereby affirming the generation of 2nd A0 waves in non-uniform plates and their applicability for local incipient damage monitoring.

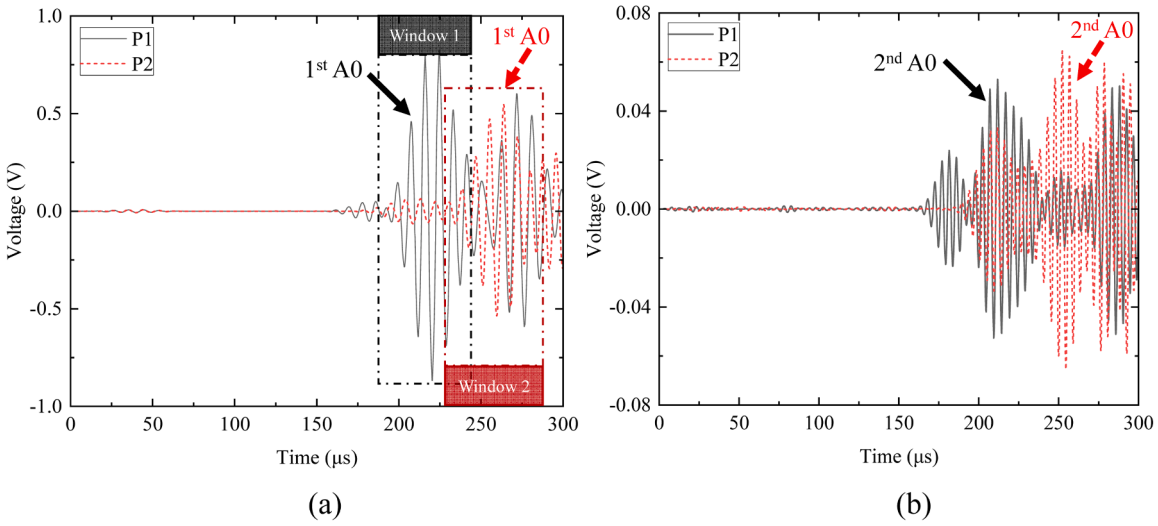

Fig. 10. The (a)linear and (b)second harmonic responses captured at P1 and P2 in the non-uniform plate.

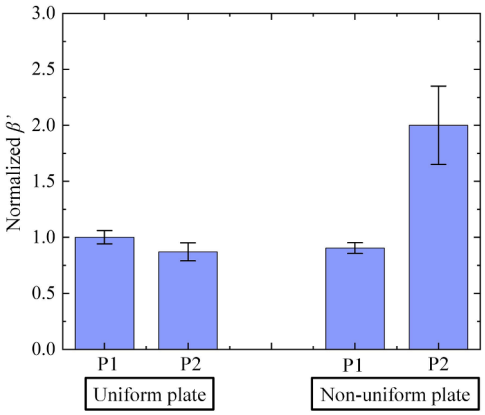

Fig. 11. Relative nonlinear parameters captured at P1 and P2 in the uniform and non-uniform plates.

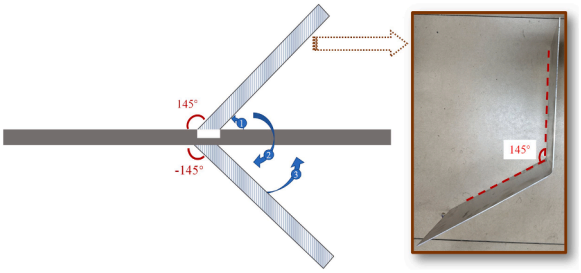

Fig. 12. Sketch of one cycle of bending for local plasticity fabrication.

5. Conclusions

This paper investigates the generation of atypical 2nd A0 mode waves in a non-uniform plate from theoretical, numerical, and experimental perspectives, in view of local incipient damage monitoring applications. It is found that the so-called atypical 2nd A0 waves can only be generated in non-uniform plates, as opposed to uniform plates, due to the interaction between incident A0 mode waves and material nonlinearity. Three different mechanisms are identified that contribute to the generation of the 2nd A0 waves: 1) the mode conversion from the 2nd S0 waves; 2) the asymmetric nonlinear driving forces at the non-uniform part; and 3) the mutual

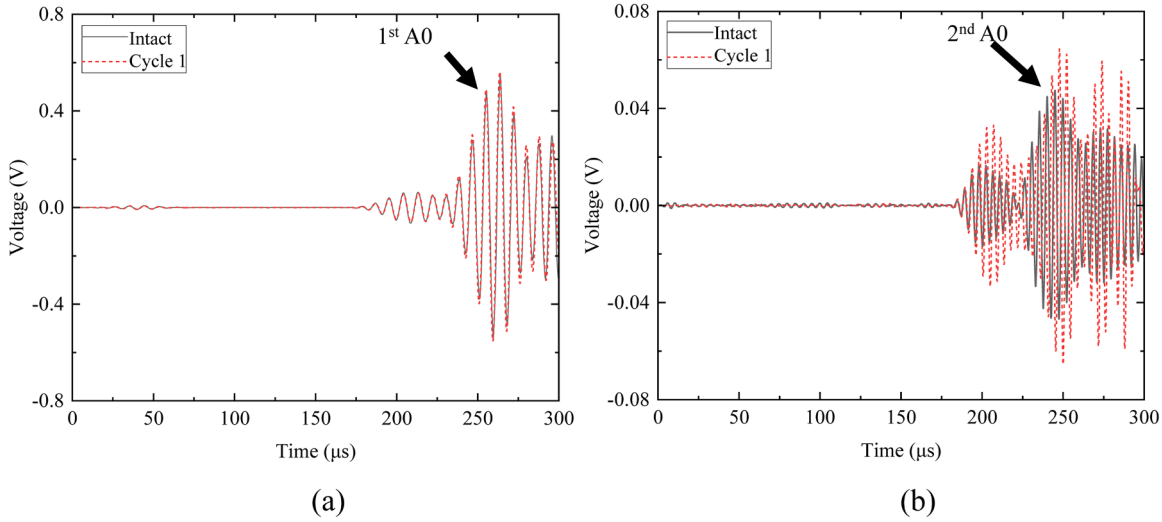

Fig. 13. The (a)linear and (b)second harmonic responses captured at P2 in the non-uniform plate before and after the 1 cycle of the bending process.

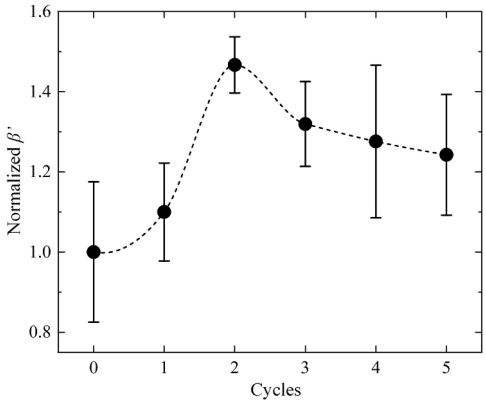

Fig. 14. Evolution of the relative acoustic nonlinear parameter in the bending process.

interaction between the mode-converted fundamental A0 and S0 waves. Despite the complex mechanisms involved, the 2nd A0 waves are only generated due to the existence of the non-uniform section. Therefore, they present great promise for monitoring local incipient damage in non-uniform structures, as demonstrated by a proof-of-concept experiment.

The findings of the present work are expected to contribute to the current state-of-the-art of the nonlinear guided wave theory and application. The revealed mechanisms for the 2nd A0 wave generation can be used to reasonably explain the complex nonlinear wave fields. In addition, the proposed local incipient damage monitoring method can also facilitate the development of the nonlinear-guided-wave-based SHM technique.

CRediT authorship contribution statement

Shengbo Shan: Writing – original draft, Methodology, Investigation, Funding acquisition, Conceptualization. **Gujun Wu:** Writing – review & editing, Validation, Investigation. **Ze Liu:** Validation, Software. **Yuanman Zhang:** Validation, Investigation. **Li Cheng:** Writing – review & editing, Supervision, Funding acquisition.

Declaration of competing interest

The authors declare that they have no known competing financial interests or personal relationships that could have appeared to influence the work reported in this paper.

Data availability

Data will be made available on request.

Acknowledgments

The work was supported by grants from the National Natural Science Foundation of China (12302114), the Research Grants Council of Hong Kong Special Administrative Region (PolyU 152013/21E), the Natural Science Foundation of Shanghai (22ZR1462700), the Fundamental Research Funds for the Central Universities, Shanghai Gaofeng Project for University Academic Program Development, and the Innovation and Technology Commission of the HKSAR Government to the Hong Kong Branch of National Rail Transit Electrification and Automation Engineering Technology Research Center (K-BBY1).

References

[1] K.H. Matlack, J.-Y. Kim, L.J. Jacobs, J. Qu, Review of second harmonic generation measurement techniques for material state determination in metals, J. Nondestruct. Eval. 34 (2015) 273, https://doi.org/10.1007/s10921-014-0273-5.
[2] V.K. Chillara, C.J. Lissenden, Review of nonlinear ultrasonic guided wave nondestructive evaluation: theory, numerics, and experiments, Opt. Eng. 55 (2015) 011002, https://doi.org/10.1117/1.OE.55.1.011002.
[3] C.J. Lissenden, Nonlinear ultrasonic guided waves—Principles for nondestructive evaluation, J. Appl. Phys. 129 (2021) 021101, https://doi.org/10.1063/5.0038340.
[4] J.C.P. Allen, C.T. Ng, Debonding detection at adhesive joints using nonlinear Lamb waves mixing, NDT E Int 125 (2022) 102552, https://doi.org/10.1016/j.ndteint.2021.102552.
[5] W. Zhu, Z. Xu, Y. Xiang, C. Liu, M. Deng, X. Qiu, D. Sun, F. Xuan, Nonlinear ultrasonic detection of partially closed cracks in metal plates using static component of lamb waves, NDT E Int 124 (2021) 102538, https://doi.org/10.1016/j.ndteint.2021.102538.
[6] C. Jiang, C. Zhang, W. Li, M. Deng, C.-T. Ng, Assessment of damage in composites using static component generation of ultrasonic guided waves, Smart Mater. Struct. 31 (2022) 045025, https://doi.org/10.1088/1361-665X/ac5a77.
[7] H. Cho, M. Hasanian, S. Shan, C.J. Lissenden, Nonlinear guided wave technique for localized damage detection in plates with surface-bonded sensors to receive Lamb waves generated by shear-horizontal wave mixing, NDT E Int. 102 (2019) 35–46, https://doi.org/10.1016/j.ndteint.2018.10.011.
[8] G. Zhao, M. Jiang, W. Li, Y. Luo, Q. Sui, L. Jia, Early fatigue damage evaluation based on nonlinear Lamb wave third-harmonic phase velocity matching, Int. J. Fatigue 167 (2023) 107288, https://doi.org/10.1016/j.ijfatigue.2022.107288.
[9] C. Jiang, W. Li, M. Deng, C.-T. Ng, Quasistatic pulse generation of ultrasonic guided waves propagation in composites, J. Sound Vib. 524 (2022) 116764, https://doi.org/10.1016/j.jsv.2022.116764.
[10] C. Yeung, C.T. Ng, Nonlinear guided wave mixing in pipes for detection of material nonlinearity, J. Sound Vib. 485 (2020) 115541, https://doi.org/10.1016/j.jsv.2020.115541.
[11] J. Wang, Y. Shen, D. Rao, W. Xu, Physical-virtual time reversing of nonlinear Lamb waves for fatigue crack detection and quantification, Mech.Syst. Sig. Process. 160 (2021), https://doi.org/10.1016/j.ymssp.2021.107921.
[12] G. Gao, C. Liu, N. Hu, M. Deng, H. Chen, Y. Xiang, Response of second-harmonic generation of Lamb wave propagation to microdamage thickness in a solid plate, Wave Motion 96 (2020) 102557, https://doi.org/10.1016/j.wavemoti.2020.102557.
[13] S. Shan, R. Ke, Y. Ma, Y. Song, L. Cheng, Quasi-phase-matched nonlinear Lamb waves in composite laminates for material degradation monitoring, NDT E Int 143 (2024) 103064, https://doi.org/10.1016/j.ndteint.2024.103064.
[14] W. Li, B. Chen, Y. Cho, Nonlinear feature of phase matched Lamb waves in solid plate, Appl. Acoust. 160 (2020) 107124, https://doi.org/10.1016/j.apacoust.2019.107124.
[15] V. Marcantonio, D. Monarca, A. Colantoni, M. Cecchini, Ultrasonic waves for materials evaluation in fatigue, thermal and corrosion damage: a review, Mech. Syst. Sig. Process. 120 (2019) 32–42, https://doi.org/10.1016/j.ymssp.2018.10.012.
[16] X. Ding, C. Xu, M. Deng, Y. Zhao, X. Bi, N. Hu, Experimental investigation of the surface corrosion damage in plates based on nonlinear Lamb wave methods, NDT E Int 121 (2021) 102466, https://doi.org/10.1016/j.ndteint.2021.102466.
[17] Y. Yang, C.-T. Ng, A. Kotousov, Second-order harmonic generation of Lamb wave in prestressed plates, J. Sound Vib. 460 (2019) 114903, https://doi.org/10.1016/j.jsv.2019.114903.
[18] W. De Lima, M. Hamilton, Finite-amplitude waves in isotropic elastic plates, J. Sound Vib. 265 (2003) 819–839, https://doi.org/10.1016/S0022-460X(02)01260-9.
[19] Y. Liu, V.K. Chillara, C.J. Lissenden, On selection of primary modes for generation of strong internally resonant second harmonics in plate, J. Sound Vib. 332 (2013) 4517–4528, https://doi.org/10.1016/j.jsv.2013.03.021.
[20] M. Deng, Cumulative second-harmonic generation of generalized Lamb-wave propagation in a solid waveguide, J. Phys. Appl. Phys. 33 (2000) 207, https://doi.org/10.1088/0022-3727/33/3/306.
[21] X. Wan, P. Tse, G. Xu, T. Tao, Q. Zhang, Analytical and numerical studies of approximate phase velocity matching based nonlinear S0 mode Lamb waves for the detection of evenly distributed microstructural changes, Smart Mater. Struct. 25 (2016) 045023, https://doi.org/10.1088/0964-1726/25/4/045023.
[22] S. Shan, L. Cheng, Mode-mixing-induced second harmonic A0 mode Lamb wave for local incipient damage inspection, Smart Mater. Struct. 29 (2020) 055020, https://doi.org/10.1088/1361-665X/ab7e37.
[23] S. Shan, L. Cheng, Two-dimensional scattering features of the mixed second harmonic A0 mode Lamb waves for incipient damage localization, Ultrasonics 119 (2022) 106554, https://doi.org/10.1016/j.ultras.2021.106554.
[24] H. Chen, M. Deng, G. Gao, C. Xu, N. Hu, Y. Xiang, Characterization of interfacial property of a two-layered plate using a nonlinear low-frequency Lamb wave approach, Ultrasonics 124 (2022) 106741, https://doi.org/10.1016/j.ultras.2022.106741.
[25] F. Masurkar, W.T. Peter, N.P. Yelve, Theoretical and experimental measurement of intrinsic and fatigue induced material nonlinearities using Lamb wave based nonlinearity parameters, Measurement 151 (2020) 107148, https://doi.org/10.1016/j.measurement.2019.107148.
[26] W. Li, J. Xiao, M. Deng, Micro-defect imaging with an improved resolution using nonlinear ultrasonic Lamb waves, J. Appl. Phys. 131 (2022) 185101, https://doi.org/10.1063/5.0087619.
[27] J. Li, M. Wang, H. Chen, P. Wang, W. Wang, Investigation on characteristics of tensile damage and microstructure evolution of steel AISI 316L by nonlinear ultrasonic Lamb wave, Int. J.Pres. Ves. Pip. 198 (2022) 104680, https://doi.org/10.1016/j.ijpvp.2022.104680.
[28] K. Balasubramaniam, S. Sikdar, T. Wandowski, P.H. Malinowski, Ultrasonic guided wave-based debond identification in a GFRP plate with L-stiffener, Smart Mater. Struct. 31 (2021) 015023, https://doi.org/10.1088/1361-665X/ac3a97.
[29] A. De Luca, D. Perfetto, G. Lamanna, A. Aversano, F. Caputo, Numerical investigation on guided waves dispersion and scattering phenomena in stiffened panels, Materials (Basel) 15 (2021) 74, https://doi.org/10.3390/ma15010074.
[30] B. Zima, R. Kędra, Detection and size estimation of crack in plate based on guided wave propagation, Mech.Syst. Sig. Process. 142 (2020) 106788, https://doi.org/10.1016/j.ymssp.2020.106788.

[31] V. Pagneux, A. Maurel, Lamb wave propagation in elastic waveguides with variable thickness, Proc. R. Soc. Lond. Ser. A Math. Phys. Eng. Sci. 462 (2006) 1315–1339, https://doi.org/10.1098/rspa.2005.1612.
[32] F.L. Feng, Y. Liu, Modal decomposition solution of Lamb wave scattering at step-like discontinuity, Adv. Mat. Res. 368 (2012) 2398–2401, https://doi.org/10.4028/www.scientific.net/AMR.368-373.2398.
[33] C. Schaal, A. Mal, Lamb wave propagation in a plate with step discontinuities, Wave Motion 66 (2016) 177–189, https://doi.org/10.1016/j.wavemoti.2016.06.012.
[34] B. Zima, J. Moll, Numerical and experimental investigation of guided ultrasonic wave propagation in non-uniform plates with structural phase variations, Ultrasonics 128 (2023) 106885, https://doi.org/10.1016/j.ultras.2022.106885.
[35] S. Sikdar, W. Ostachowicz, A. Kundu, Deep learning for automatic assessment of breathing-debonds in stiffened composite panels using non-linear guided wave signals, Compos. Struct. 312 (2023) 116876, https://doi.org/10.1016/j.compstruct.2023.116876.
[36] D.D. Mandal, S. Banerjee, Identification of breathing type disbonds in stiffened panels using non-linear lamb waves and built-in circular PWT array, Mech.Syst. Sig. Process. 117 (2019) 33–51, https://doi.org/10.1016/j.ymssp.2018.07.040.
[37] W. Zuo, Z. An, B. Zhang, Z. Hu, Solution of nonlinear Lamb waves in plates with discontinuous thickness, J. Acoust. Soc. Am. 155 (2024) 2171–2180, https://doi.org/10.1121/10.0025382.
[38] S. Shan, M. Hasanian, H. Cho, C.J. Lissenden, L. Cheng, New nonlinear ultrasonic method for material characterization: codirectional shear horizontal guided wave mixing in plate, Ultrasonics 96 (2019) 64–74, https://doi.org/10.1016/j.ultras.2019.04.001.
[39] S. Shan, L. Cheng, P. Li, Adhesive nonlinearity in Lamb-wave-based structural health monitoring systems, Smart Mater. Struct. 26 (2016) 025019, https://doi.org/10.1088/1361-665X/26/2/025019.
[40] X. Sun, G. Shui, Y. Zhao, W. Liu, N. Hu, M. Deng, Evaluation of early stage local plastic damage induced by bending using quasi-static component of Lamb waves, NDT E Int. 116 (2020) 102332, https://doi.org/10.1016/j.ndteint.2020.102332.
[41] Z. Liu, S. Shan, L. Cheng, Nonlinear-Lamb-wave-based plastic damage detection assisted by topologically designed metamaterial filters, Struct. Health Monit. 22 (2023) 1828–1843, https://doi.org/10.1177/14759217221114525.